Nanoscale Mapping of the Mechanical Properties of Polymer Surfaces by Means of AFM Noise Analysis: Spatially Resolved Fibrillation of Latex Films

ARTICLE *in* LANGMUIR · NOVEMBER 2003

Impact Factor: 4.46 · DOI: 10.1021/la034924m · Source: OAI

3 AUTHORS, INCLUDING:

Farida Benmouna
Abou Bakr Belkaid University of Tlemcen
49 PUBLICATIONS **455** CITATIONS
SEE PROFILE

Tatiana Dimitrova
Dow Corning Corporation
14 PUBLICATIONS **261** CITATIONS
SEE PROFILE

Nanoscale Mapping of the Mechanical Properties of Polymer Surfaces by Means of AFM Noise Analysis: Spatially Resolved Fibrillation of Latex Films

Farida Benmouna,† Tatiana D. Dimitrova, and Diethelm Johannsmann*

Max-Planck-Institute for Polymer Research, Ackermannweg 10, 55128 Mainz, Germany

Received May 28, 2003. In Final Form: September 4, 2003

Polymer latex surfaces were investigated with a new instrument performing mechanical imaging based on the thermal motion of a cantilever of an atomic force microscope. In low-viscosity environments, the power spectral density of the cantilever's Brownian motion is given by resonance curves. From the resonance frequency, the bandwidth, and the amplitude, one obtains the effective spring constant and the drag coefficient of the cantilever. These parameters change when the cantilever makes contact with the sample and provide information on the sample's mechanical properties. The instrument has three-channel nanopositioning capability with feedback-control. The noise power spectra are analyzed in real-time. The imaging capabilities were employed to correlate the surface topography of polymer latex films with the film's ability to produce filaments on pulling with the AFM tip. The film surface has a granular structure due to incomplete coalescence of the neighboring particles. The micromechanical properties of elongated filaments depend on the spatial position of the AFM tip. Most filaments originate from the center of the underlying particle. The mechanical properties of the filaments as a function of pulling distance are characterized by plateaus and steps.

Introduction

The atomic force microscope is increasingly used to perform mechanical studies on the molecular scale. Widely known are single molecule force spectroscopy,[1] shear force modulation,[2] friction microscopy,[3] force modulation,[4] and—on a slightly less quantitative basis—the "tapping mode".[5] Pertinent to most of these techniques is a problem of linear response of the sample. Perturbations which would be considered truly minute in conventional mechanical spectroscopy easily damage the sample when applied across an AFM tip. This argument applies to forces as well as displacements. A force of 1 nN is beyond the damage threshold of many soft objects if the force acts across a square nanometer (corresponding to a pressure of 1 GPa). An extension of 1 nm is more than what many small molecules can withstand without rupturing.

For soft materials, an analysis based on the fluctuation dissipation theorem provides an alternative. As Einstein has stated early in the last century, the diffusion coefficient of a particle is inversely proportional to the viscosity in its environment.[6] Thermal diffusion, by nature, is a gentle process. While it is not strictly guaranteed that thermal diffusion never leaves the range of linear response, it is true in most cases of practical interest. Linear response in this context means that the force is proportional to the displacement (or the speed) at all times. Exceptions from linear behavior are rare.[7] Via the Einstein relation the diffusion of a probe particle provides access to the local viscosity. The extension of this approach to viscoelastic materials has been extensively discussed in the context of light scattering[8] and single particle tracking[9] on colloidal dispersions. The technique has also been used in a biological context.[10]

Here we report on a conceptually related approach, where the fluctuating object is not a colloidal sphere but rather the cantilever of an atomic force microscope (AFM).[11−15] The analysis of the data is very similar to the data treatment in single-particle nanorheology. Although the present work follows this concept, the two approaches differ in a number of respects. First, the AFM tip can only access surfaces, whereas colloidal particles can be located anywhere in the bulk. Second, the precise positioning of the AFM tip is relatively easy. Colloidal particles can be positioned with an optical[16,17] or a magnetic[18] tweezer. However, this is a complicated task. Often, nanorheology is performed without active positioning of the probe.

* Author for correspondence. Present address: Institute of Physical Chemistry, Technical University Clausthal, Arnold-Sommerfeld-Str. 4, D-38678 Clausthal-Zellerfeld, Germany. Phone: +49 (0)-5323-72 3768. Fax: +49 (0)-5323-72 4835. E-mail: johannsmann@pc.tu-clausthal.de.

† On leave from Macromolecular Research Laboratory, Faculty of Sciences, University Aboubakr Belkaid, Tlemcen BP 119, Algeria.

(1) Clausen-Schaumann, H.; Seitz, M.; Krautbauer, R.; Gaub, H. E. *Curr. Opin. Chem. Biol.* **2000**, *4*, 524.

(2) Ge, S.; Pu, Y.; Zhang, W.; Rafailovich, M.; Sokolov, J.; Buenviaje, C.; Buckmaster, R.; Overney, R. M. *Phys. Rev. Lett.* **2000**, *85*, 2340.

(3) Kajiyama, T.; Tanaka, K.; Ohki, I.; Ge, S. R.; Yoon, J. S.; Takahara, A. *Macromolecules* **1994**, *27*, 7932.

(4) Radmacher, M.; Tillmann, R. W.; Gaub, H. E. *Biophys. J.* **1993**, *64*, 735.

(5) Mallegol, J.; Dupont, O.; Keddie, J. L. *Langmuir* **2001**, *17*, 7022.

(6) Einstein, A. *Ann. Phys.* **1906**, *19*, 371.

(7) Hoh, J. H.; Cleveland, J. P.; Prater, C. B.; Revel, J. P.; Hansma, P. K. *J. Am. Chem. Soc.* **1992**, *114*, 4917.

(8) Dasgupta, B. R.; Tee, S. Y.; Crocker, J. C.; Frisken, B. J.; Weitz, D. A. *Phys. Rev. E* **2002**, *65*, 051505.

(9) (a) Crocker, J. C.; Valentine, M. T.; Weeks, E. R.; Gisler, T.; Kaplan, P. D.; Yodh, A. G.; Weitz, D. A. *Phys. Rev. Lett.* **2000**, *85*, 888. (b) MacKintosh, F. C.; Schmidt, C. F. *Curr. Opin. Colloid Interface Sci.* **1990**, *4*, 300. (c) Strick, T.; Allemand, J. F.; Croquette, V.; Bensimon, D. *Prog. Biophys. Mol. Biol.* **2000**, *74*, 115.

(10) Tseng, Y.; Kole, T. P.; Wirtz, D. *Biophys. J.* **2002**, *83*, 3162.

(11) Roters, A.; Gelbert, M.; Schimmel, M.; Rühe, J.; Johannsmann, D. *Phys. Rev. E* **1997**, *56*, 3256.

(12) Gelbert, M.; Biesalski, M.; Rühe, J.; Johannsmann, D. *Langmuir* **2000**, *16*, 5774.

(13) Butt, H. J.; Jaschke, M.; Ducker, W. *Bioelectrochem. Bioenerg.* **1995**, *38*, 191.

(14) Sader, J. E. *J. Appl. Phys.* **1998**, *84*, 1.

(15) Schäffer, T. E.; Cleveland, J. P.; Ohnesorge, F.; Walters, D. A.; Hansma, P. K. *J. Appl. Phys.* **1996**, *80*, 3622.

(16) Tischer, C.; Altmann, S.; Fisinger, S.; Horber, J. K. H.; Stelzer, E. H. K.; Florin, E.-L *Appl. Phys. Lett.* **2001**, *79*, 3878.

(17) Pralle, A.; Florin, E. L.; Stelzer, E. H. K.; Horber, J. K. H. *Appl. Phys. A* **1998**, *66*, S71.

(18) Bausch, A. R.; Moller, W.; Sackmann, E. *Biophys. J.* **1999**, *76*, 573.

10.1021/la034924m CCC: $25.00
Published on Web 10/30/2003

Third, the AFM tip is elastically suspended, whereas the colloidal particles diffuse freely. In the case of the AFM, the noise power spectrum is a resonance curve. The surface properties are inferred from the shift of the resonance parameters.

Further, the AFM is more sensitive, because it is based on the optical lever technique. The detection electronics of the AFM easily picks up motions on the scale of 1 Å, whereas the limit for conventional microscopy is somewhere around a few nanometers. This increased accuracy can be traced back to the use of a mirror which is much larger than the tip. In principle, the sensitivity of both conventional optics and the optical lever technique is limited by diffraction. The smaller the divergence of the laser beam at the mirror, the more accurate the determination of beam deflection. The internal divergence, on the other hand, is about equal do λ/D with λ the wavelength of light and D the diameter of mirror. Since D can be much larger than λ (and much larger than a typical colloidal particle), sensitivity is gained. Connecting the object of interest (the tip) to a larger mirror amounts to an amplification scheme.

Finally, the mirror provides a gain in sensitivity, but of course, the interaction between the tip and the sample may be affected by the (much larger) cantilever, as well. These effects are most prominent in liquids. In air, hydrodynamics is less important. Just as in conventional atomic force microscopy, long-range hydrodynamic effects adversely affect the spatial resolution.

One might think that an imaging mode of AFM noise analysis would be prohibitively slow. That is not necessarily the case. Below we provide a calculation of the minimum time for data acquisition. The central parameters are the resonance frequency and the bandwidth. In the experiments reported below, the resonance frequency is about 50 kHz, and the bandwidth is 3 kHz or more. To reliably determine the resonance frequency, the spectral resolution must be better than the inverse bandwidth of the cantilever. A resolution of 1 kHz is sufficient. According to the sampling theorem,[19] data acquisition for a single spectrum with a resolution of 1 kHz takes 0.5 ms. Within 1 s, one can accumulate 2000 spectra, resulting in a signal-to-noise ratio for each data point of $2000^{1/2} \sim 45$. This accuracy easily suffices for the measurements reported below. In liquids the bandwidth of the cantilever increases and the rate of the data acquisition can be increased accordingly. Assuming a rate of data acquisition of one spectrum per second, one straightforwardly calculates that an image of 100 pixels × 100 pixels takes about 3 h. Given these time scales, one has to fight thermal drifts of the scanner. However, there are various schemes of feedback-control. In the investigation reported here, we just allowed for good thermal equilibration in a closed compartment.

Actually, one can speed up the measurement by a factor of about 100 by sacrificing spectral resolution and just basing the measurement of the spring constant on the rms noise, $\kappa \approx k_B T/\langle \delta z^2 \rangle$, via the equipartition theorem. The latter states that each degree of freedom contributes $^1/_2 k_B T$ to the time-averaged energy. The fundamental oscillation counts as a single degree of freedom. The higher modes of deflection are excluded by only considering frequencies below 100 kHz.

In this fast mode of data acquisition the drag coefficient is unavailable. Also, it turns out that the rms noise is somewhat plagued by problems of calibration such as a slightly variable optical lever sensitivity or the detector leaving the linear range. Therefore, we do not pursue this approach here. Resonance frequency and bandwidth are entirely unaffected by these problems and therefore provide a much cleaner access to the mechanical parameters of the system.

In this communication we show that an imaging mode of AFM noise analysis is perfectly feasible. It is a simple add-on to the existing AFM setups and provides a wealth of information unavailable with other techniques.

Theoretical Background

The noise power spectrum of the cantilever motion can be used to probe the viscoelastic properties of its environment.[20,21] Within the model of the simple harmonic oscillator, the statistical motion of an elastically suspended particle is described by the Langevin equation:

$$m \frac{d^2 z(t)}{dt^2} + \xi \frac{dz(t)}{dt} + \kappa z(t) = R(t) \qquad (1)$$

where z is the displacement, m the effective mass, ξ the drag coefficient, κ the spring constant, and $R(t)$ the random force. All of these are "effective" parameters, including the cantilever's interaction with the substrate. For example, the spring constant increases when the cantilever touches a substrate.[20]

In the simple-harmonic-oscillator approximation, the power spectrum, $|\delta z(\omega)^2|$, is given by resonance curves of the form[14,15]

$$|\delta z(\omega)^2| = 2k_B T \frac{\xi}{(\kappa - m\omega^2)^2 + \xi^2 \omega^2} = 2k_B T \frac{\gamma}{m} \frac{1}{({\omega_0}^2 - \omega^2)^2 + \gamma^2 \omega^2} \qquad (2)$$

with $k_B T$ the thermal energy, $\omega_0 = (\kappa/m)^{1/2}$ the resonance frequency, and $\gamma = \xi/m$ the width of the resonance. The time-averaged displacement of the cantilever $\langle \delta z \rangle$ (proportional to the static force, F_{DC}) is always measured, in parallel. The parameters m, κ, and ξ are the results of fitting the spectra with eq 2.

In liquids it turns out that the simple harmonic approximation sometimes fails. We deal with this situation by treating the drag coefficient as a complex frequency-dependent quantity. The function $\xi'(\omega)$ can be explicitly derived from the noise power spectra. The software has the capability to carry out this analysis in real-time. This work was carried out in air, where the benefit is an increased lateral resolution due to the absence of long-range hydrodynamic interactions. In air, the resonances are rather sharp and a frequency-dependence of κ and ξ does not enter in the analysis. Since the entire information is contained in the resonances, the parameters frequency and bandwidth capture the behavior well.

Experimental Setup and Data Acquisition

Figure 1 shows a sketch of the setup. The instrument consists of a commercial AFM head (Topometrix), which is fixed to a metal base. The latter in screwed to a three-channel piezoelectric flexure stage for fine approach, allowing for a travel range of 100 × 100 × 20 μm^3 (P-517.3CL from Physik Instrumente, Karlsruhe, Germany). The piezo stage has active feedback-control with capacitive sensors for distance control (E-500.50). Actually, the

(19) Press, W. H.; Teukolsky, S. A.; Vetterling, W. T.; Flannery, B. P. *Numerical Recipes in Pascal*; Cambridge University Press: 1990.

(20) Roters, A.; Johannsmann, D. *J. Phys.: Condens. Matter* **1996**, *8*, 7561.

(21) See, for example: Kubo, R.; Toda, M.; Hashitsume, H. *Statistical Physics*; Springer: Heidelberg, 1985; Vol. 2.

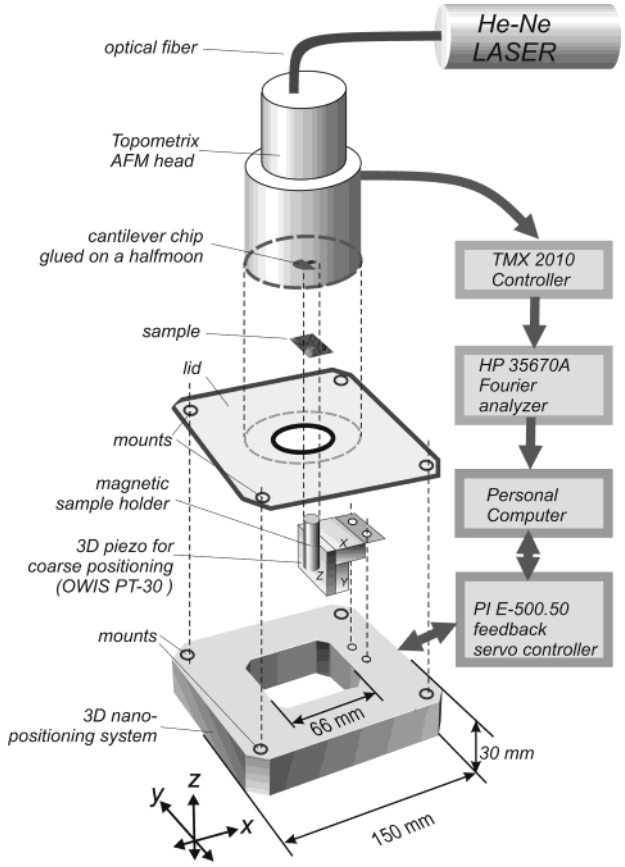

Figure 1. Sketch of the experimental configuration for AFM noise based imaging (not to scale).

feedback mechanism coming into action whenever the sample is moved significantly contributes significantly to the total time needed for taking an image.

A magnetic sample holder is attached to an *xyz* inertia drive for the coarse approach (PT30, OWIS, Staufen, Germany). This assembly is fixed to the three-channel piezo stage. To minimize thermal drift, the setup is situated in a closed chamber. Although there is a table for active vibration isolation, such measures proved to be unnecessary. The experiment can be performed either in air or in liquid. The experiments were carried out at room temperature without active control of temperature.

The laser diode of the AFM head was replaced by a HeNe laser connected to the AFM head with a single mode optical fiber. This modification reduces nonthermal noise connected to the pointing instability of the laser diode.[22] The noise power spectra are acquired with a Fourier analyzer (HP 35670A) connected to the analog output of the quadrant detector. Two hundred spectra were accumulated for each position of the cantilever.

The control of the experiment, the data acquisition, and the analysis are done with home-written software. The software has a built-in function for calibration of the optical lever sensitivity from the force−distance curves on hard surfaces. The spectra are on-line fitted with resonance curves. The derivation of a frequency-dependent drag coefficient $\xi'(\omega)$ can also be done in real-time. This option only applies to measurements in liquids. Raw spectra are not usually saved. However, one can save the raw data and reanalyze them at a later stage. Such a reanalysis may make sense because the analysis needs certain parameters (like the fitting range) affecting the outcome of the fit.

The cantilever chip is glued to a half-moon mount which is held with magnets on the AFM head. The angle between the cantilever and the surface is 15°. Since the Fourier analyzer has a maximum frequency of 100 kHz, the resonance frequency of the cantilever must remain well below this limit.

(22) Cleveland, J. P.; Schaffer, T. E.; Hansma, P. K. *Phys. Rev. B* **1995**, *52*, R8692.

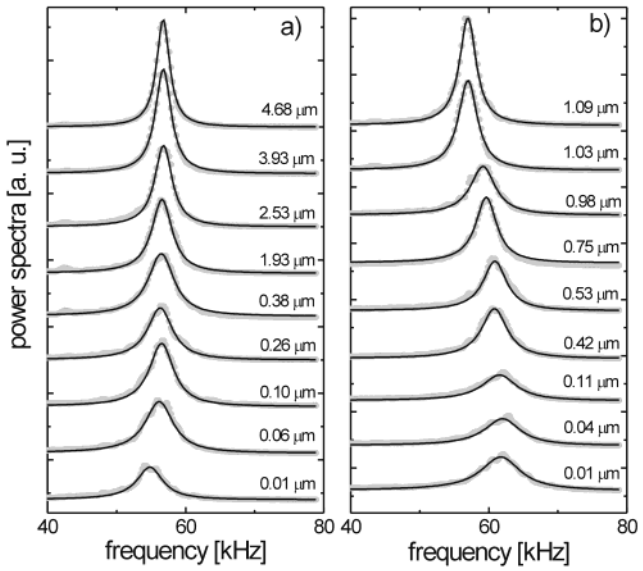

Figure 2. Noise power spectra density (gray dots) and corresponding fits with resonance curves: (a) approach; (b) retraction.

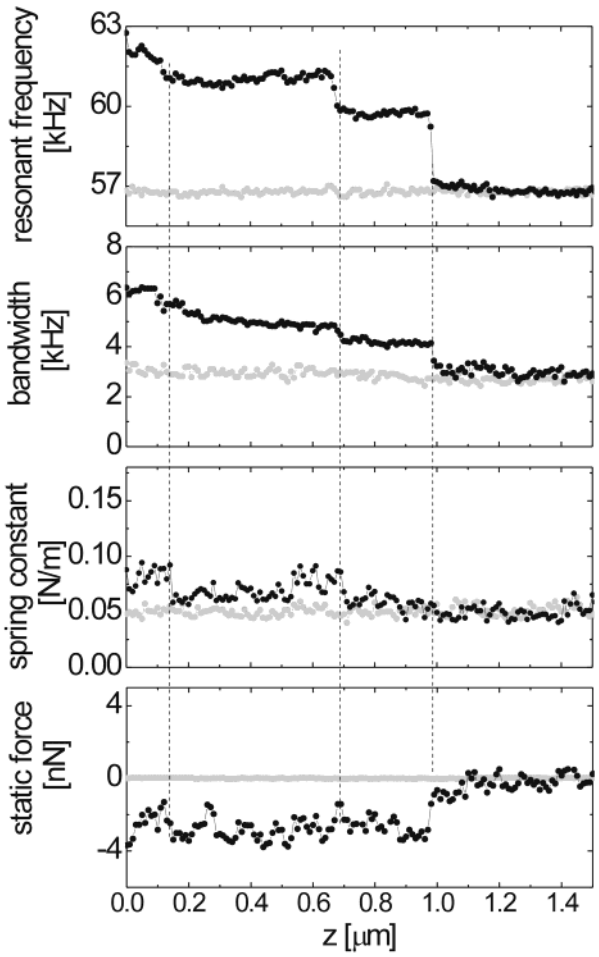

Figure 3. Representative data set showing the variation of resonant frequency, bandwidth, spring constant, and static force with vertical displacement. Black and gray dots correspond to a "successful" and an "unsuccessful" pull, respectively.

The calibration of the spring constant of the cantilever is usually done far from the surface either from the root-mean-square displacement (using the equipartition theorem), or, alternatively, by a Lorentz fit to the spectrum. The values derived with both methods agree well.

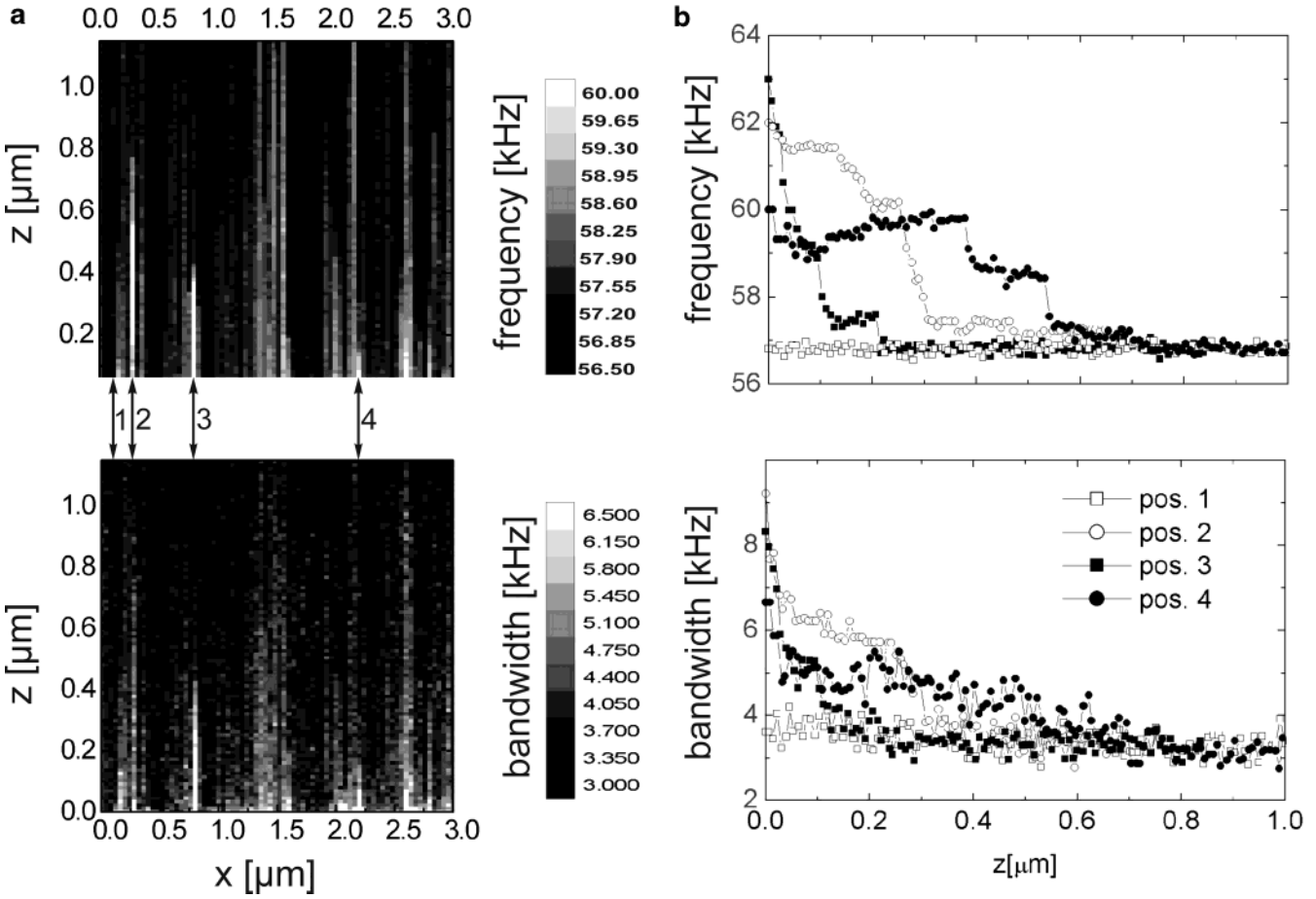

Figure 4. (a) 2D plot of the resonance frequency (top) and resonance bandwidth (bottom), recorded on retraction. Brighter stripes correspond to filaments elongated between the AFM tip and the polymer film. (b) Resonance frequency (top) and resonance bandwidth (bottom), at $x = 0.08$ μm (position 1), $x = 0.28$ μm (position 2), $x = 0.80$ μm (position 3), and $x = 2.20$ μm (position 4). Position 1 corresponds to the case where no filament is elongated (unsuccessful pull).

One of the most severe problems is the suppression of nonthermal noise. Electronic noise at discrete frequencies is easily noticed and can be eliminated by excluding these (narrow) frequency ranges from the fits. A second measure is a "watch dog" which rejects noisy spectra *before* accumulation on the basis of the integral (rms) noise. Nonthermal noise will always increase (often very substantially) the total noise. Below a frequency of about 0.5 kHz we observe that the fluctuation power is proportional to the inverse of the frequency. This effect is the well-known $1/f$ noise which we cannot avoid. The exact origin of the $1/f$ noise is under debate. It has electronic contributions but probably contains other disturbances as well. These low-frequency data have to be discarded entirely.

To obtain a 2D map of the viscoelastic parameters in the (x, z) plane, the following procedure is used: after bringing the sample to a distance of a few microns from the sample surface with the coarse control, one initiates an automated scan in one vertical ("z") dimension and one lateral ("x") dimension. 3D scans are possible but very time-consuming. At a given lateral position, the sample is vertically approached to the probe. For each step the noise spectra of the cantilever are recorded and the data are on-line analyzed. Usually, the direction of motion is reversed after firm contact has been established, where "firm contact" can either mean (depending on the sample) a jump into contact as evidenced by a sudden attractive force or a strong repulsive force. After each cycle of approach and retraction the lateral position is incremented and another approach−retraction cycle is initiated. The instrument also allows for making scans on approach only, in which case the piezo returns directly to its initial position right after contact. One can save time by skipping data points where the tip and the sample are clearly out of contact (black areas in Figure 4).

Materials and Sample Preparation

The images shown below were obtained on a dried film of a polyacrylate dispersion. The dispersion was provided by BASF AG, Ludwigshafen, Germany. The material was synthesized by emulsion polymerization. The mean particle diameter (obtained by dynamic light scattering) is 300 nm. The properties are optimized for application as pressure sensitive adhesives. Details of chemical composition are proprietary. In a previous study we have shown that filaments may be drawn from this material upon a gentle contact of an AFM tip with the surface of the film.[23] Furthermore, the films maintain the granular structure (with clearly distinguishable disperse and continuous phases) even after extended aging.

The substrates (standard microscope slides) were cleaned by 15 min sonication in ionic detergent (2% Hellmanex, HELLMA, Germany), followed by 20 min sonication in deionized water, washing with MilliQ water, and drying in nitrogen. Films with a (wet) thickness of 10 μm were formed with a pulling blade (Erichsen, Germany, model 97065 or 94060). The samples were dried at room temperature for 24 h. The surface of the dried films was then gently washed with deionized water. After washing, the films were again dried for 24 h and stored desiccated. The aging of the films was achieved only by storage. The term "time after preparation" used hereafter refers to the time elapsed after the second drying step.

AFM micrographs were taken with a NanoScope III atomic force microscope (Digital Instruments, Inc, Santa Barbara, CA) equipped with a J or E scanner. All films were imaged in ambient atmosphere, at 22 °C in tapping mode. We used Ultrasharp silicon probes (MikroMach, Estonia, model CSC12) with a resonance

(23) Dimitrova, T. D.; Johannsmann, D.; Willenbacher, N.; Pfau, A. *Langmuir* **2003**, *19*, 5748.

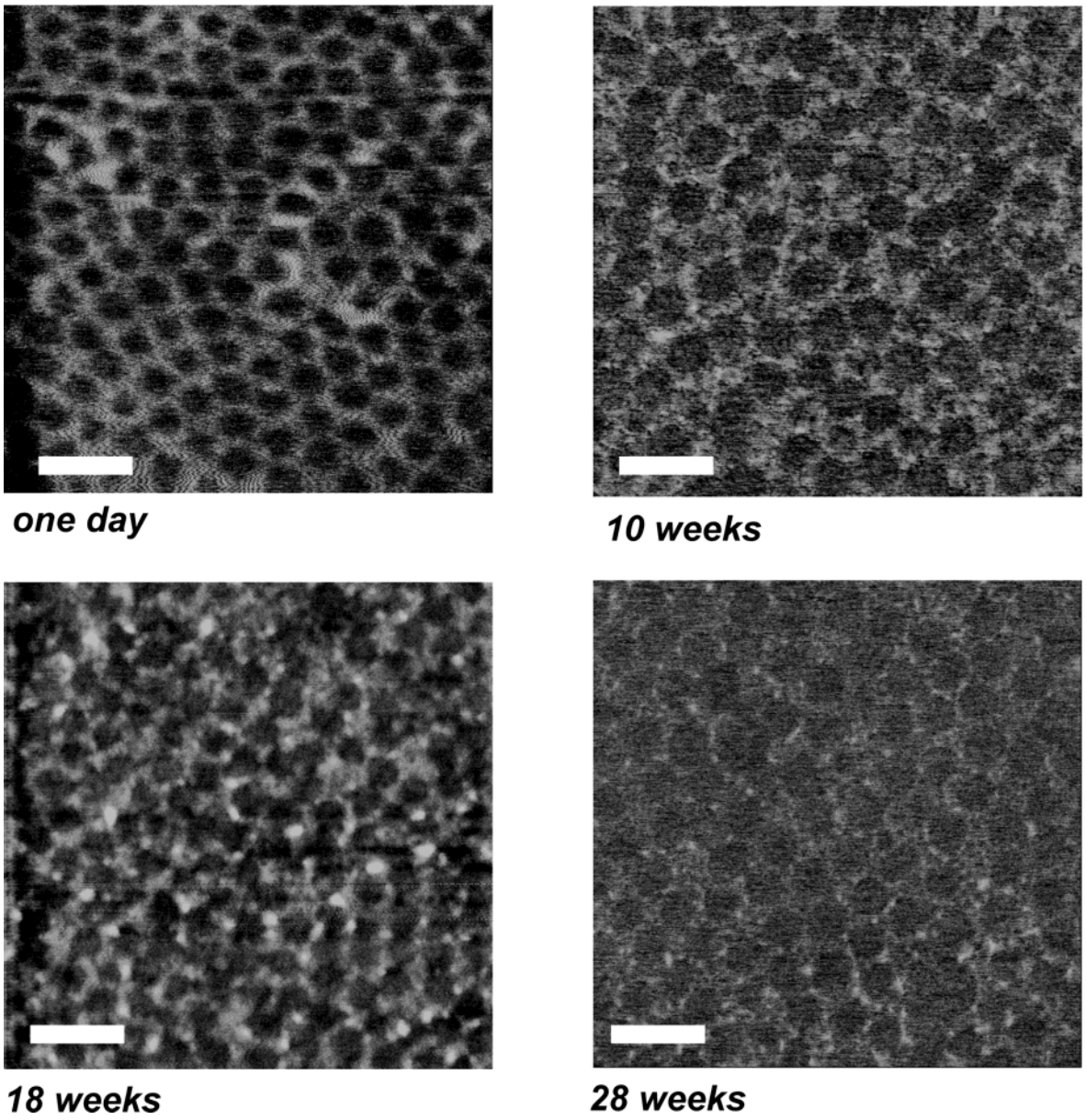

Figure 5. Time evolution of the surface morphology (phase images recorded in tapping mode). The bar is 1 μm in all cases.

frequency of about 170 kHz and a spring constant (manufacturer information) of 1.75 N/m. In tapping mode (intermittent contact) the cantilever is oscillated near its resonance frequency, with an amplitude high enough to overcome the adhesive forces.[24] At least three images at randomly chosen locations were obtained for each aging step.

After bringing the sample to a distance of about 5 μm from the cantilever with the coarse control, an automated scan in the $x-z$ plane was run. The increments were 40 nm in the lateral dimension and 10 nm in the vertical dimension. When the tip jumps into contact with the film, the direction of scan is reversed. It is necessary to choose the vertical range large enough to allow for complete separation between two cycles of approach.

Since all the parameters extracted from the noise spectra reflect the entire system of the cantilever in its environment, it is important to perform all experiments with *one and the same cantilever*. We used a V-shaped silicone nitride cantilever (Digital Instruments, CA) with a length $L = 100$ μm, a resonance frequency (in air) of 56.7 kHz, and a bandwidth, Δf_{HBFW}, of 2 kHz. The spring constant κ was determined as 0.06 N/m by use of the equipartition theorem. Only the fundamental resonance frequency was visible in the experimental frequency window of 1−100 kHz (Figure 2).

(24) Sheiko, S. *Adv. Polym. Sci.* **2000**, *151*, 61.

Results and Discussion

Figure 2 shows typical power spectra (dots) and the fits with resonance curves (lines) as a function of the vertical piezo travel. The change of the resonance curve reflects changes of the mechanical properties of the tip−sample system. On retraction (Figure 2b) the resonance frequency is increased, indicating an increased spring constant. Note that the increased bandwidth in these curves is *not* a consequence of hydrodynamic damping. It is caused by the filaments bridging the gap between the surface and the tip. A small amount of hydrodynamic damping is observed on approach, as shown in Figure 2a.

Thermal drifts necessitate a leveling procedure. The z-values in the raw data are moved such that neighboring vertical lines are displaced relative to each other. We redefine the origin of the z-scale on the basis of the outcome of the measurements. Evidently, any topographical information is lost in this flattening step. On retraction, we have chosen $z = 0$ to coincide with the position at which the strong adhesion between the tip and the film is overcome and the first resonance curve is resolved. We only show data for retraction here; the data for approach are entirely trivial.

Figure 3 shows the resonance frequency, the bandwidth, the spring constant (calculated from the equipartition theorem), and the static force for two x positions as a function of the piezo

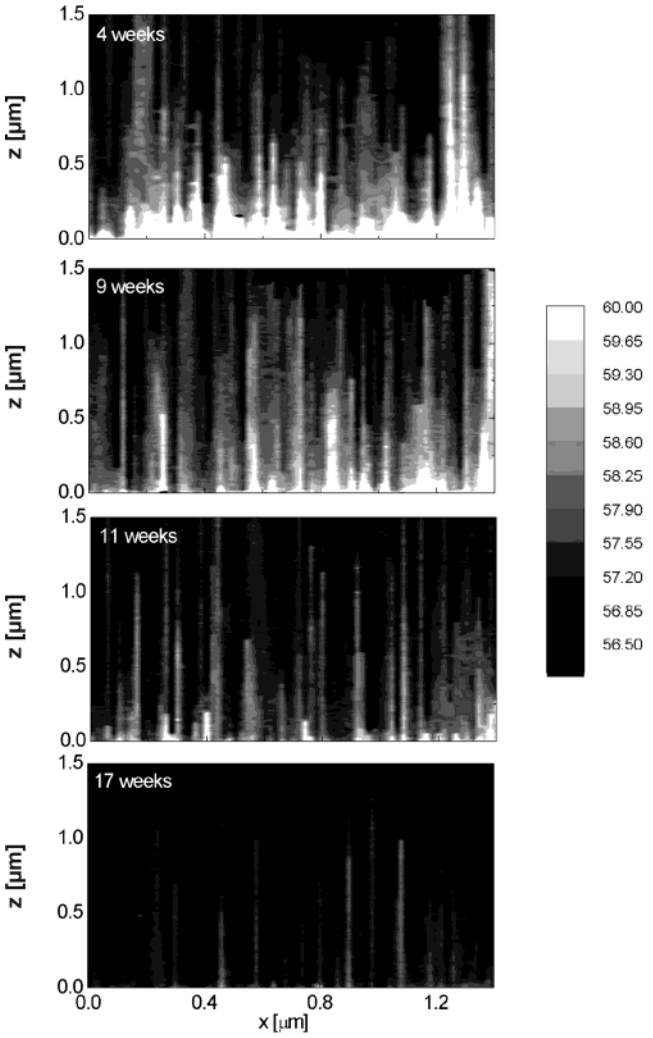

Figure 6. Time evolution of the mechanical properties of the investigated filaments.

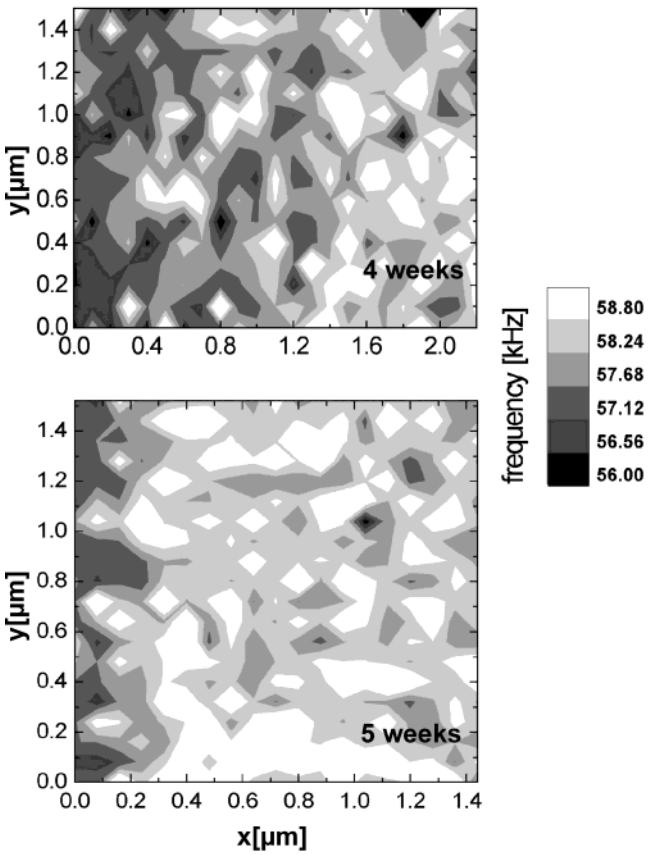

Figure 7. Surface plot of the resonance frequency recorded on retraction. The data are taken 20 nm above the initiation of the pulling. Brighter parts correspond to filaments; black areas correspond to unsuccessful pulls (see text for details).

z-travel. Data are taken while the sample is retracted. The data show a large variability. The black dots correspond to a case were a filament has been successfully picked up and elongated for about 1 μm. The gray symbols correspond to what we call an "unsuccessful pull". In this case no filament is drawn out of the film and the tip jumps out of contact immediately. All the parameters resume the values corresponding to those of the free cantilever right then. This difference is the basis for the quantification of the fibrillation ability of the material. The likelihood of drawing a filament out of the film is correlated with the position and the age of the sample.

As seen from Figure 3, the resonance frequency is the quantity with the smallest scatter. We therefore mainly use the resonance frequency for building maps. The bandwidth may be used as well (cf. parts a and b of Figure 4). The resonance frequency is closely related to the spring constant. The quantitative conversion between resonance frequency and spring constant suffers from the fact that the amplitude of the thermal noise enters ($\kappa = \omega_0^2 m$, where the effective mass, m, is related to the amplitude). The amplitude, however, fluctuates rather strongly for reasons not related to the sample. Maps of the spring constant as a consequence do not provide the same degree of spatial resolution as maps of the resonance frequency.

Figure 4a shows a 2D plot of the resonance frequency. Figure 4b shows the bandwidth recorded simultaneously with the resonance frequency. Both images correlate well. The steps of displacement were 40 and 20 nm in x and z, respectively. The data are taken on films which had been aged for 6 weeks.

The majority of the filaments extend over a distance of about 1 μm. This is larger than the previously observed extension of 250 nm.[23] In fact, the experimental conditions are different due to the intrinsic features of the two instruments. First, in ref 23 the cantilever was slowly and continuously approached to the surface, which enabled us to detect the jump into contact *without* allowing the tip to penetrate into the film. In the present experiment the tip approaches the surface of the film by steps of 10 nm. As a consequence, each tip−sample contact leads to indentation with a depth of up to 20 nm and an increased contact area. Second, the contact time varied from <1 s in ref 23 to at least 2 s here. The time lag is necessary for the feedback positioning. The larger contact area and longer contact of the tip with the film may result in longer filaments. We recall that the material has been optimized for application as pressure sensitive adhesives. Therefore, it wets many surfaces well.

The behavior of the elongated filaments may follow different scenarios. As Figure 4b shows, during the elongation, the resonant frequency (i.e. the elastic strength) of each filament undergoes several transitions. This behavior is attributed to the consecutive rupture of interparticle junctions, which exist between the individual particles in the film and in the filament.[23]

The elongation rates in the two experiments are similar, being 2 nm/s in ref 23 and 1.5 nm/s here, which permits the comparison of the mechanical properties of the elongated filaments.

The filaments (brighter vertical lines in Figure 4a) are grouped with respect to the lateral coordinate with a period of about 0.4 μm, which corresponds reasonably well to the size of the individual spheres constituting the film. AFM imaging was performed on the same samples.

Figure 5 shows the evolution of the surface morphology with aging. Only the phase images are shown. Evidently, the fusion of latices is incomplete even after 28 weeks of storage.

Figure 6 summarizes the change of the film fibrillation with time. Note that different spots on the sample are investigated. The x positions in the different images do not correspond to each other. Both the number of the filament and their average length decrease with time.

Given the granular structure of the films, the data in Figure 4 suggest the existence of preferential zones for formation of

filaments. However, these preferential locations of filament formations could be either the center of the particle or the interstices. The question of whether filaments mostly originate from the particle center or the rim can only be decided on the basis of a 3D map. A full 3D map, on the other hand, is prohibitively time-consuming. A compromise is a quasi-2D map in the surface plane, where each pull is interrupted once the data allow the statement on whether the pull was successful or not. Such a decision can be based on the resonance frequency of a few spectra. If this resonance frequency is increased, a filament is pulled; otherwise, the tip has snapped off. In Figure 7 we plot the resonance frequency at the very beginning of the pulling, recorded during (x, y, z) scans. We plot only the resonance frequency corresponding to $z = 20$ nm, where $z = 0$ is the position where a clear resonance spectrum is discernible for the first time. This distance is sufficient to ensure the absence of capillary effects due to water condensation, and at the same time it allows for a reliable statement on whether a filament was formed. The graphs represent the lateral distribution of the filaments along the surface of a sample aged for 4 weeks and 5 weeks; black areas correspond to "unsuccessful pulls". The images are taken at two different locations of the film. As seen from the image, there are large bright areas, which could be associated with the individual particles (as opposed to dark spots, which would correspond to interstitial areas).

Conclusions

We have constructed an instrument based on AFM noise analysis, which allows for local mechanical imaging. It was employed to study the mechanical properties of the filaments formed when the AFM tip is withdrawn from the surface of polymer films. The latter were formed from industrial polyacrylic latices and preserve their granular structure even after extended aging. We report on images in (x, z) and (x, y) planes. On the basis of these maps, we demonstrate that the micromechanical properties of the elongated filaments as well as their length depend on the spatial position of the AFM tip. Most of the filaments originate from the center of the particles. The fibrillation ability depends on the age of the films as well. With aging the coalescence between the neighboring particles increases, which results in lowering of the fibrillation ability.

Acknowledgment. F.B. thanks the Alexander von Humboldt Foundation for financial support. T.D.D. has been supported by a Marie Curie Fellowship of the European Community program "Human Potential" under Contract Number HPMF-CT-2001-01188. The authors thank Dr. Norbert Willenbacher and Dr. Andreas Pfau from BASF AG for providing the samples and for the stimulating discussions.

LA034924M